Spectral Element Method for Modeling Eccentric Coaxial Waveguides Filled with Anisotropic Media via Conformal Transformation Optics

Raul O. Ribeiro[#1], Johnes R. Gonçalves[#], Fernando L. Teixeira[$], José R. Bergmann[#], Guilherme S. Rosa[#2]
[#]Center for Telecommunications Studies, PUC-Rio, Rio de Janeiro, RJ, Brazil
[$]ElectroScience Laboratory, The Ohio State University, Columbus, OH, USA
[1]raul.ribeiro@cetuc.puc-rio.br, [2]guilhermeSimonDaRosa@cetuc.puc-rio.br

***Abstract* — In this work, a spectral element method (SEM) in cylindrical coordinates is explored for analyzing the electromagnetic field propagation in eccentric coaxial waveguides filled with anisotropic media. The proposed formulation employs conformal transformation optics to map the original problem into an equivalent concentric coaxial waveguide. Our novel cylindrical-coordinate-based SEM facilitates the mapping between reference and curvilinear elements for waveguides that present cylindrical-conforming boundaries. The proposed approach was validated against perturbation and finite-difference-based solutions, and preliminary results show that our solution excels because of its accuracy and low computational cost. With a few adaptations, the present cylindrical SEM formulation can be extended for modeling a large class of problems involving complex media such as metamaterial devices and geophysical exploration sensors.**

***Keywords* — Anisotropic media, conformal transformation optics, eccentric coaxial waveguide, spectral element method.**

I. Introduction

The study of electromagnetic propagation in coaxial waveguides with an offset in the center conductor is essential in several applications such as sensing probes, microwave filters, geophysical exploration, and the medical industry [1]–[3]. Several approaches have been developed to determine the cutoff wavenumbers of the propagation modes in these structures. In [4], conformal mapping was used to transform the eccentric coaxial cross-section into an equivalent problem covering a rectangular domain. In [5], cylindrical harmonic functions were combined with Graf's theorem to model the effect of small eccentricities. In [6], the Helmholtz equation was solved in a bipolar coordinate system (BCS) by the separation of variables. In [7], transformation optics principles were employed to map the eccentric problem into an equivalent concentric problem, and the cutoff wavenumbers were obtained using perturbation techniques.

The spectral element method (SEM) has been applied successfully to a large variety of electromagnetic problems [8]–[10]. The work [10] indicates that the SEM formulation based on cylindrical coordinates requires considerably fewer elements and degrees of freedom (DoF) than the conventional Cartesian approach for cylindrical-conforming geometries. With this in mind, the present work applies transformation optics to map the original eccentric waveguide problem into an equivalent concentric one similar to [7] but here with no restrictions on the eccentricity offset. The cylindrical SEM is then employed for the solution of the mapped problem.

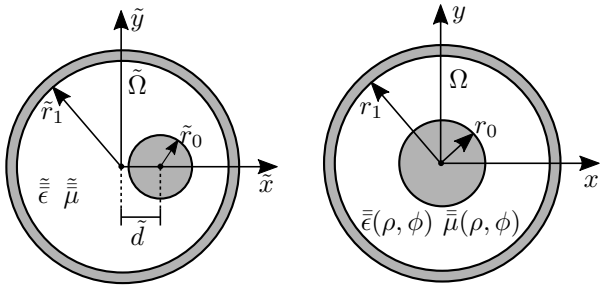

Fig. 1. (a) Cross-section $\tilde{\Omega}$ of an eccentric coaxial waveguide. (b) Cross-section Ω of a concentric coaxial waveguide.

II. Formulation Overview

A. Variational Waveguide Problem

Consider an eccentric coaxial waveguide invariant along the axial direction. The eccentric geometry is referred to as a cylindrical coordinate system denoted by $(\tilde{\rho}, \tilde{\phi}, \tilde{z})$. The associated cross-section $\tilde{\Omega}$ is depicted in Fig. 1a. The inner circular cylinder with radius $\tilde{r}_0$ is a perfect electric conductor (PEC) with an offset $\tilde{d}$ from the $\tilde{z}$-axis. The outer cylinder is represented by a PEC at $\tilde{r}_1$. The waveguide is filled with a uniaxially anisotropic medium characterized by complex permeability $\tilde{\bar{\mu}} = \text{diag}(\tilde{\mu}_s, \tilde{\mu}_s, \tilde{\mu}_z)$ and permittivity $\tilde{\bar{\epsilon}} = \text{diag}(\tilde{\epsilon}_s, \tilde{\epsilon}_s, \tilde{\epsilon}_z)$ tensors. From conformal transformation optics principles [11]–[13], the original electromagnetic problem in the eccentric coordinates $(\tilde{\rho}, \tilde{\phi}, \tilde{z})$ can be transformed into a concentric problem with coordinates (ρ, ϕ, z) using

$$\mathbf{F} = \bar{\bar{J}} \cdot \tilde{\mathbf{F}}, \ \text{ with } \ \mathbf{F} \in \{\mathbf{E}, \mathbf{H}\}, \tag{1}$$

$$\bar{\bar{p}} = |\bar{\bar{J}}|^{-1} \bar{\bar{J}} \cdot \tilde{\bar{\bar{p}}} \cdot \bar{\bar{J}}^T, \ \text{ with } \ p \in \{\mu, \epsilon\}, \tag{2}$$

where $\bar{\bar{J}}$ is the Jacobian of the transformation $(\tilde{\rho}, \tilde{\phi}, \tilde{z}) \rightarrow (\rho, \phi, z)$. Assuming $\tilde{z} = z$ and $\tilde{r}_1 = r_1$, we can express the transformed constitutive tensors as [13]

$$\bar{\bar{p}} = \text{diag}(p_s, p_s, p_z(\rho, \phi)) = \text{diag}(\tilde{p}_s, \tilde{p}_s, |\bar{\bar{J}}|^{-1} \tilde{p}_z), \tag{3}$$

with $p \in \{\mu, \epsilon\}$, where

$$|\bar{\bar{J}}|^{-1} = \frac{(1 - \tilde{x}_1/\tilde{x}_2)^2}{(1 - 2\rho\cos\phi/\tilde{x}_2 + \rho^2/\tilde{x}_2^2)^2}, \tag{4}$$

$$\tilde{x}_{1,2} = \frac{-c \mp \sqrt{c^2 - 4\tilde{r}_1^2}}{2}, \ \text{ with } \ c = \frac{\tilde{r}_0^2 - \tilde{r}_1^2 - \tilde{d}^2}{\tilde{d}}. \tag{5}$$

The problem in Ω-domain (depicted in Fig. 1b) can be solved by decomposing electromagnetic fields into a sum of transverse magnetic (TM) and transverse electric (TE) modes [14, Ch. 5]. It is convenient to solve E_z and H_z axial field components and then compute the transverse components of the fields in cylindrical coordinates. The wave equation for E_z and H_z in the concentric scenarios satisfies

$$\left(\nabla_s^2 + \frac{p_z(\rho,\phi)}{p_s} k_\rho^2\right) F = 0, \tag{6}$$

where ∇_s^2 is the transverse Laplacian operator, k_ρ is the radial wavenumber, $F = E_z$ if $p_{s,z} = \epsilon_{s,z}$, and $F = H_z$ if $p_{s,z} = \mu_{s,z}$. Using the Galerkin method [15], we can write the variational formulation for problem (6) as

$$\langle \boldsymbol{\nabla}_s F, \boldsymbol{\nabla}_s W\rangle - k_\rho^2 \left\langle \frac{p_z(\rho,\phi)}{p_s} F, W \right\rangle = 0, \tag{7}$$

where the brackets denote an inner product in Hilbert space, $F \in \{E_z, H_z\}$, and $W \in C_c^\infty(\Omega)$.

B. Spectral Element Method

Our computational domain is first discretized by four elements Ω^e covering the entire coaxial waveguide cross-section Ω as shown in Fig. 2. Each element is described by the polar coordinates (ρ, ϕ), which is then mapped into the reference coordinates (ξ, η) via

$$\rho^e(\xi) = 0.5(\rho_0^e + \rho_1^e) + 0.5(\rho_1^e - \rho_0^e)\xi, \ \ \forall \xi \in [-1,1], \tag{8a}$$

$$\phi^e(\eta) = 0.5(\phi_0^e + \phi_1^e) + 0.5(\phi_1^e - \phi_0^e)\eta, \ \ \forall \eta \in [-1,1]. \tag{8b}$$

The mapping above allows us to relate the transverse points of the reference element covering $-1 \le \xi \le 1$ and $-1 \le \eta \le 1$ with the physical element covering $\rho_0^e \le \rho \le \rho_1^e$ and $\phi_0^e \le \phi \le \phi_1^e$. The associated Jacobian matrix of this coordinate transformation is given by

$$\bar{\bar{J}}_s^e = \begin{bmatrix} \frac{\partial \rho^e}{\partial \xi} & \frac{\partial \rho^e}{\partial \eta} \\ \rho \frac{\partial \phi^e}{\partial \xi} & \rho \frac{\partial \phi^e}{\partial \eta} \end{bmatrix} = \begin{bmatrix} 0.5(\rho_1^e - \rho_0^e) & 0 \\ 0 & 0.5\rho(\phi_1^e - \phi_0^e) \end{bmatrix}. \tag{9}$$

Note that the Jacobian is diagonal, consequently, ρ- and η-directions are decoupled, and directions ϕ and ξ are also decoupled [10].

To represent the field components in the reference coordinates, we use Lagrange basis functions associated with Gauss-Lobatto-Legendre (GLL) sampling points. For example, with the sampling points $\xi_k \in [-1,1]$, for all $j = 1, 2, ..., N+1$, along the coordinate ξ, the Nth-order one-dimensional GLL basis function is given by

$$\phi_j^N(\xi) = \prod_{k \ne j}^{N+1} \frac{\xi - \xi_k}{\xi_j - \xi_k} \ \ \forall \xi \in [-1,1], \tag{10}$$

where the $N+1$ interpolation nodes ξ_k are the roots of the $(N+1)$-degree completed Lobatto polynomial $(1-\xi^2)Lo_{N-1}(\xi) = 0$. Accordingly, the two-dimensional GLL basis function is obtained via tensor-product expansions

$$\hat{\psi}_{ij}(\xi,\eta) = \phi_i^N(\xi)\phi_j^N(\eta) \ \ \forall (\xi,\eta) \in [-1,1]^2. \tag{11}$$

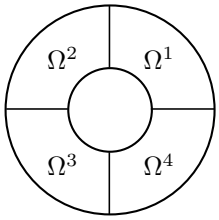

Fig. 2. Discretization of a coaxial domain Ω into four elements.

On the other hand, the corresponding basis function ψ_{ij}^e and its gradient in the physical element can be obtained by the covariant mappings [15]

$$\begin{cases} \psi_{ij}^e(\rho,\phi) = \hat{\psi}_{ij}(\xi,\eta) \\ \boldsymbol{\nabla}_s \psi_{ij}^e(\rho,\phi) = \bar{\bar{J}}_s^{e\,-1} \hat{\boldsymbol{\nabla}}_s \hat{\psi}_{ij}(\xi,\eta) \end{cases}, \tag{12}$$

where $\boldsymbol{\nabla}_s = \left(\frac{\partial}{\partial\rho}, \frac{1}{\rho}\frac{\partial}{\partial\phi}\right)^T$, $\hat{\boldsymbol{\nabla}}_s = \left(\frac{\partial}{\partial\xi}, \frac{\partial}{\partial\eta}\right)^T$. The Jacobian matrix $\bar{\bar{J}}_s^e$ is defined by (9), and $|\bar{\bar{J}}_s^e|$ denotes its determinant.

To construct the discrete form of problem (7), the axial field F in the reference domain is expanded as

$$F(\xi,\eta) = \sum_{n=1}^{(N+1)^2} a_n \hat{\psi}_n(\xi,\eta). \tag{13}$$

Following the Galerkin method, test functions are identical to the basis functions, $W = \hat{\psi}_m$ for $m = 1, 2, ..., (N+1)^2$. Using (13) and (12), we can define elemental matrices that represent the inner products in (7). These matrices can be written in reference coordinates as

$$\mathbf{D}^e(m,n) = \int_{-1}^{1}\int_{-1}^{1} (\bar{\bar{J}}_s^{e\,-1} \hat{\boldsymbol{\nabla}}_s \hat{\psi}_n)^T \cdot (\bar{\bar{J}}_s^{e\,-1} \hat{\boldsymbol{\nabla}}_s \hat{\psi}_m) |\bar{\bar{J}}_s^e| d\xi d\eta, \tag{14a}$$

$$\mathbf{M}^e(m,n) = \int_{-1}^{1}\int_{-1}^{1} \frac{p_z(\rho(\xi),\phi(\eta))}{p_s} \hat{\psi}_n \cdot \hat{\psi}_m |\bar{\bar{J}}_s^e| d\xi d\eta. \tag{14b}$$

The integrands in (14) are evaluated using the Gauss-Lobatto quadrature [16]. The global diffusion matrix $\mathbf{D}$ and global mass matrix $\mathbf{M}$ are assembled via elemental matrices $\mathbf{D}^e$ and $\mathbf{M}^e$, for $e \in \{1,2,3,4\}$, respectively. Next, we define the generalized eigenvalue problem

$$\mathbf{D}\bar{a} = k_{\rho c}^2 \mathbf{M}\bar{a}, \tag{15}$$

where $k_{\rho c}^2$ and $\bar{a}$ are the eigenvalues and eigenvectors. The eigenvalues are associated with the radial cutoff wavenumbers, while the eigenvectors are associated with the axial field coefficients in (13).

III. Numerical Results

As our first validation, we consider an eccentric waveguide with $\tilde{r}_1 = 5$ mm, $\tilde{r}_0 = 0.05\tilde{r}_1$, and offset $\tilde{d} = 0.05\tilde{r}_1$, assuming the background medium as the vacuum. This problem was considered before in [6], [7] and is chosen here to evaluate the accuracy of our SEM-based technique. Table 1 shows the cutoff wavenumbers $k_{\rho c}$

Table 1. Cutoff wavenumbers were obtained by the FEM from [17], BCS from [6], CMPM and RPM from [7], and our SEM-based technique. The relative percentage errors ε (%) were calculated using the dense-mesh FEM solution as a reference.

	FEM	BCS		CMPM		RPM		SEM	
Mode	$k_{\rho c}$ (m^{-1})	$k_{\rho c}$ (m^{-1})	ε (%)	$k_{\rho c}$ (m^{-1})	ε (%)	$k_{\rho c}$ (m^{-1})	ε (%)	$k_{\rho c}$ (m^{-1})	ε (%)
TE_{11}	366.156	367.226	0.292	367.789	0.446	366.230	0.020	366.370	0.058
TE_{21}	610.692	612.837	0.351	611.333	0.105	610.796	0.017	610.800	0.017
TE_{31}	840.159	842.354	0.261	843.861	0.441	840.234	0.009	840.235	0.009
TM_{01}	610.692	614.559	0.633	614.109	0.559	610.674	0.003	611.070	0.061
TM_{11}	775.540	774.038	0.194	774.695	0.109	775.698	0.020	775.662	0.032
TM_{21}	1027.331	1029.802	0.241	1028.743	0.137	1027.383	0.005	1027.386	0.006

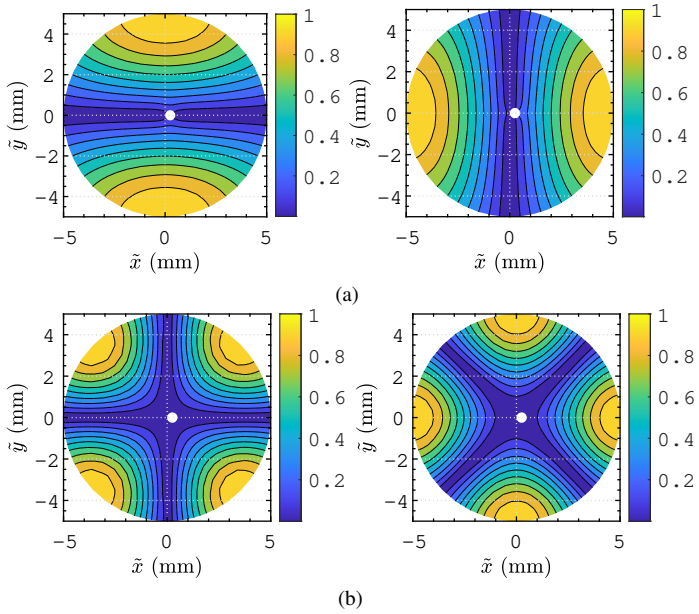

Fig. 3. Pair of normalized axial magnetic fields H_z for (a) TE_{11} and (b) TE_{21} modes obtained by SEM.

for the first three TE and TM modes obtained by (a) dense-mesh FEM from CST Studio [17], (b) BCS from [6], (c) cavity-material perturbation (CMPM) and (d) regular perturbation method (RPM) both from [7], and (e) the proposed SEM using expansion functions of order $N = 7$. The relative percentage error ε (%) was defined using the dense-mesh FEM solution as reference. All methods show good agreement, but the errors observed in BCS and CMPM approaches are considerably larger than in the RPM and SEM counterparts. An advantage of SEM compared to RPM is the ability to obtain a pair of eigenvalues associated with the symmetry planes of the problem at hand. Fig. 3 shows pairs of normalized axial magnetic field patterns for the TE_{11} and TE_{21} configurations. In addition, the accuracy of SEM can be improved by increasing the expansion order N regardless of the eccentricity, while the accuracy of RPM perturbation formulas in [7] degrades as the eccentricity increases.

Given the same waveguide as before, now we investigate the accuracy of the SEM solutions considering different eccentricity offsets $\tilde{d} \in \{0.05\tilde{r}_1, 0.10\tilde{r}_1, 0.15\tilde{r}_1, 0.20\tilde{r}_1\}$. Fig. 4 shows the cutoff wavenumber of the first three TE and TM modes as a function of the normalized offset $\tilde{d}/\tilde{r}_1$ using

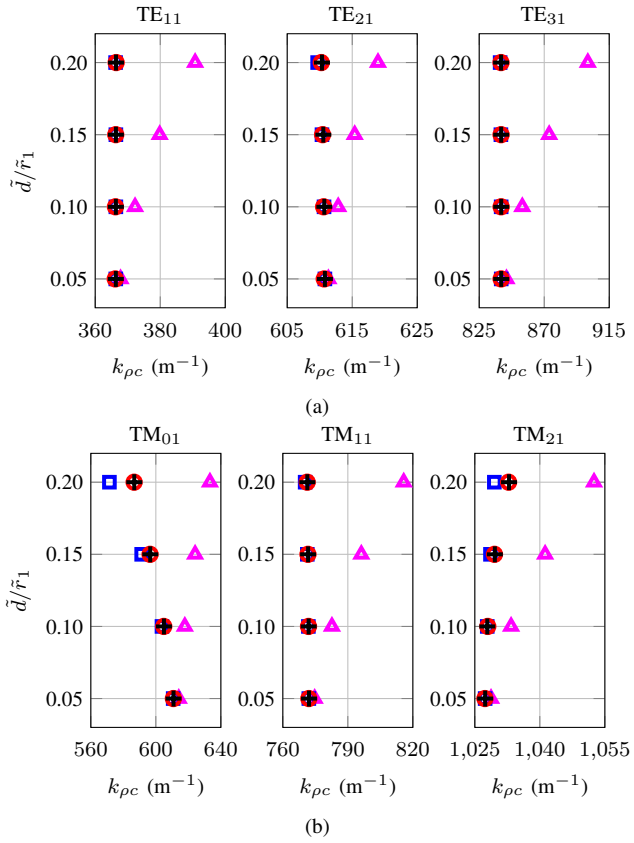

Fig. 4. Cutoff wavenumbers for (a) TE and (b) TM modes as a function of the normalized eccentricity distance $\tilde{d}/\tilde{r}_1$ get by CMPM (△), by RPM (□), by FEM (○), and by SEM (+).

FEM from [17], CMPM and RPM from [7], and the present SEM-based approach. Notice that CMPM does not yield results for larger offsets $\tilde{d} \geq 0.1\tilde{r}_1$. In particular, the TM_{01} and TM_{21} results from RPM present a noticeable error for $\tilde{d} = 0.2\tilde{r}_1$. In all simulated cases, the SEM showed excellent agreement compared to the FEM reference solution, which indicates that this approach can be extended to geometries that present a more significant offset of the inner conductor.

Finally, we investigate the ability of our SEM formulation to solve eccentric waveguides filled with anisotropic media. For this, we reproduce the cases considered in [7], in which $\tilde{\epsilon}_s = \epsilon_0\tilde{\epsilon}_{rs}$, $\tilde{\epsilon}_z = \epsilon_0\tilde{\epsilon}_{rz}$, and $\tilde{\mu}_s = \tilde{\mu}_z = \mu_0$, where ϵ_0 and μ_0 are the vacuum values. The geometry has $\tilde{r}_1 = 5$ mm, $\tilde{r}_0 = 0.05\tilde{r}_1$, and offset $\tilde{d} = 0.2\tilde{r}_1$. Figs. 5 and 6 show results for the

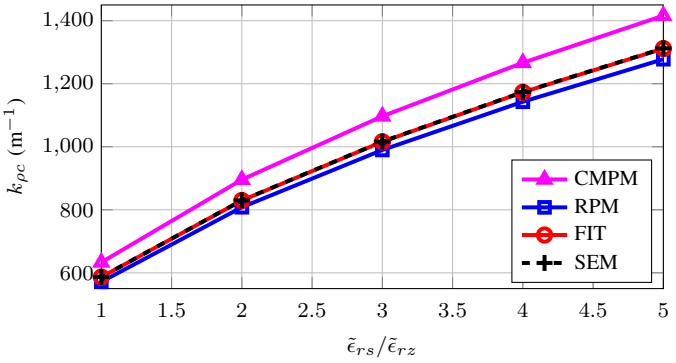

Fig. 5. Cutoff wavenumbers for the TM_{01} mode as a function of the anisotropic permittivity ratio $\tilde{\epsilon}_{rs}/\tilde{\epsilon}_{rz}$, with $\tilde{\epsilon}_{rz} = 1$.

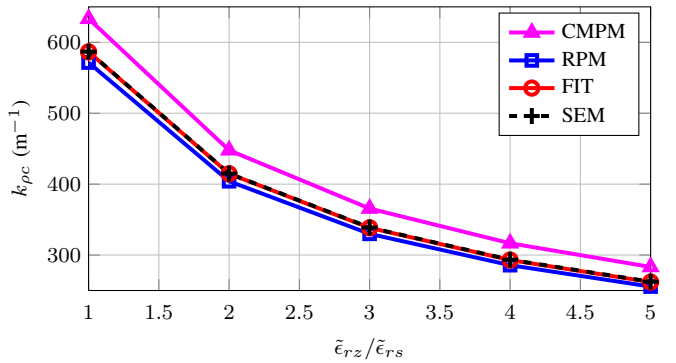

Fig. 6. Cutoff wavenumbers for the TM_{01} mode as a function of the anisotropic permittivity ratio $\tilde{\epsilon}_{rz}/\tilde{\epsilon}_{rs}$, with $\tilde{\epsilon}_{rs} = 1$.

Table 2. Computational cost.

	FIT	CMPM	RPM	SEM
Case I	15 min 44 s	2.07 s	16.72 s	6.37 s
Case II	22 min 27.10 s	2.43 s	21.60 s	6.37 s

cutoff wavenumbers of the TM_{01} mode as a function of $\tilde{\epsilon}_{rs}$ and $\tilde{\epsilon}_{rz}$. We use dense-mesh finite-integration technique (FIT) [17] results as reference. We can observe that the SEM outperforms both the CMPM and RPM.

The computational time cost required by the SEM (expansion function of order $N = 7$) is compared with that of the FIT, CMPM, and RPM in Table 2 for the anisotropic waveguide with $\tilde{\epsilon}_{rs} = 5$ and $\tilde{\epsilon}_{rz} = 1$ (Case I), with $\tilde{\epsilon}_{rz} = 5$ and $\tilde{\epsilon}_{rs} = 1$ (Case II). The present SEM shows excellent computational performance compared to the other techniques, considering also that the CMPM does provide a similar level of accuracy. The SEM-based algorithms were written in the MATLAB [18] environment running on a PC with 2.90 GHz Intel Core i7-10700 with eight cores.

IV. Conclusion

This work has investigated a novel SEM in cylindrical coordinates for solving the modal fields in eccentric coaxial waveguides filled with uniaxially anisotropic media. The proposed formulation employs transformation optics to map the original problem into an equivalent concentric coaxial problem. The SEM results showed excellent agreement with dense-mesh reference FEM and FIT solutions, at a considerably lower computational cost.

References

[1] M. Razmhosseini, R. Zabihi, and R. G. Vaughan, "Wideband antennas using coaxial waveguide," *IEEE Trans. Antennas Propag.*, vol. 69, no. 10, pp. 6273–6283, 2021.

[2] G. Xing, H. Xu, and F. L. Teixeira, "Evaluation of eccentered electrode-type resistivity logging in anisotropic geological formations with a matrix method," *IEEE Trans. Geosci. Remote Sens.*, vol. 56, no. 7, pp. 3895–3902, 2018.

[3] R. Herschmann and O. Büchel, "Radiation characteristics of a coaxial waveguide with eccentric inner conductor for application in hyperthermia and microwave reflex therapy," *Advances in Radio Science*, vol. 5, no. BK, pp. 189–195, 2007.

[4] H. Yang and S. Lee, "A variational calculation of te and tm cutoff wavenumbers in circular eccentric guides by conformal mapping," *Microwave and Optical Technology Letters*, vol. 31, no. 5, pp. 381–384, 2001.

[5] A. D. Kotsis and J. A. Roumeliotis, "Cutoff wavenumbers of eccentric circular metallic waveguides," *IET Microwaves, Antennas & Propagation*, vol. 8, no. 2, pp. 104–111, 2014.

[6] M. Gholizadeh, M. Baharian, and F. H. Kashani, "A simple analysis for obtaining cutoff wavenumbers of an eccentric circular metallic waveguide in bipolar coordinate system," *IEEE Trans. Microw. Theory Techn.*, vol. 67, no. 3, pp. 837–844, 2019.

[7] J. R. Gonçalves, G. S. Rosa, and F. L. Teixeira, "Perturbative analysis of anisotropic coaxial waveguides with small eccentricities via conformal transformation optics," *IEEE Trans. Microw. Theory Techn.*, vol. 69, no. 9, pp. 3958–3966, 2021.

[8] N. Liu, G. Cai, C. Zhu, Y. Tang, and Q. H. Liu, "The mixed spectral-element method for anisotropic, lossy, and open waveguides," *IEEE Trans. Microw. Theory Techn.*, vol. 63, no. 10, pp. 3094–3102, 2015.

[9] J. Liu, W. Jiang, N. Liu, and Q. H. Liu, "Mixed spectral-element method for the waveguide problem with bloch periodic boundary conditions," *IEEE Trans. Electromagn. Compat.*, vol. 61, no. 5, pp. 1568–1577, 2019.

[10] R. O. Ribeiro, G. S. Rosa, and J. R. Bergmann, "An improved formulation of the spectral element method in cylindrical coordinates for the analysis of anisotropic-filled waveguide devices," in *2022 IEEE International Symposium on Antennas and Propagation and USNC-URSI Radio Science Meeting (AP-S/URSI)*, 2022, pp. 1526–1527.

[11] F. Teixeira and W. Chew, "Differential forms, metrics, and the reflectionless absorption of electromagnetic waves," *Journal of Electromagnetic Waves and Applications*, vol. 13, no. 5, pp. 665–686, 1999.

[12] L. Xu and H. Chen, "Conformal transformation optics," *Nature Photonics*, vol. 9, pp. 15–23, 01 2015.

[13] G. S. Rosa, J. R. Bergmann, F. L. Teixeira, and M. S. Novo, "A perturbation-based method to model electromagnetic logging sensors in eccentric boreholes via conformal transformation optics," in *12th Eur. Conf. Antennas Propag. (EuCAP)*, 2018, pp. 1–5.

[14] R. F. Harrington, *Time-harmonic electromagnetic fields*. McGraw-Hill College, 1961.

[15] P. Monk *et al.*, *Finite element methods for Maxwell's equations*. Oxford University Press, 2003.

[16] C. Pozrikidis, *Introduction to Finite and Spectral Element Methods using MATLAB*. Chapman & Hall Book, 2014.

[17] CST AG, CST Studio Suite 2019, Darmstadt, Germany, 2019.

[18] *MATLAB version 9.12.0.2009381 (R2022a) Update 4*, The Mathworks, Inc., Natick, Massachusetts, 2022.